

# Complex singularities around the QCD critical point at finite densities

Shinji Ejiri\*

*Graduate School of Science and Technology,  
Niigata University, Niigata 950-2181, Japan*

Yasuhiko Shinno<sup>†</sup>

*Nara National College of Technology,  
Yamatokoriyama, Nara 639-1080, Japan*

Hiroshi Yoneyama<sup>‡</sup>

*Department of Physics, Saga University,  
Saga 840-8502, Japan*

(Dated: November 11, 2021)

## Abstract

Partition function zeros provide alternative approach to study phase structure of finite density QCD. The structure of the Lee-Yang edge singularities associated with the zeros in the complex chemical potential plane has a strong influence on the real axis of the chemical potential. In order to investigate what the singularities are like in a concrete form, we resort to an effective theory based on a mean field approach in the vicinity of the critical point. The crossover is identified as a real part of the singular point. We consider the complex effective potential and explicitly study the behavior of its extrema in the complex order parameter plane in order to see how the Stokes lines are associated with the singularity. Susceptibilities in the complex plane are also discussed.

---

\*Electronic address: ejiri@muse.sc.niigata-u.ac.jp

<sup>†</sup>Electronic address: shinno@libe.nara-k.ac.jp

<sup>‡</sup>Electronic address: yoneyama@cc.saga-u.ac.jp

## I. INTRODUCTION

The critical point (CP) [1–5] of QCD at finite temperatures and densities is an important issue, and its existence and associated nature of the quark gluon plasma phase may be clarified by the heavy ion experiments in the near future [6]. This is one of the main targets lattice simulations are aiming at. The situation is, however, not conclusive due to the notorious sign problem. Various approaches such as the Taylor series [7–10] and the imaginary chemical potential [11–17] are adopted in order to circumvent the sign problem [18–20]. Their validity is controlled by the thermodynamic singularities in the complex chemical potential plane [21, 22]. Such singularities are deeply associated with the partition function zeros. In [23], the QCD singularities have been investigated in the complex  $\mu$  plane by using  $N_f = 2$  QCD with staggered quarks. In the present paper, we pursue this issue in terms of an effective theory, by focusing on the singularities in the vicinity of the CP in the complex chemical potential plane.

Study of the partition function zeros [21, 24–36] provides an alternative approach to the critical phenomena and its scaling behaviors. The partition function as a function of parameter  $\lambda$  such as temperature and magnetic field for finite volume takes zero at  $\lambda = \lambda_k$  in the complex  $\lambda$  plane.

$$Z(\lambda) = \prod_k (\lambda - \lambda_k).$$

As pointed out by Lee-Yang [25], there is an analogy with two dimensional Coulomb gas. In the infinite volume limit, the zeros accumulate on curves  $C$  with a “charge density”  $\xi(s)$ , and the real part of the free energy  $\Omega(\lambda)$  becomes

$$\text{Re } \Omega(\lambda) = -T \int_C ds \xi(s) \log |\lambda - \lambda(s)|. \quad (1)$$

$\text{Re } \Omega$  is continuous across  $C$ , while the “electric field”  $\mathbf{E} = -\nabla \text{Re}(\Omega)$  is discontinuous in the direction normal to the curve. The amount of the discontinuity is proportional to the charge density  $\xi$ . This curve named as the Stokes line is regarded as the location of a cut on a Riemann sheet of the analytic function  $\text{Re}\Omega$ . It should be noted that the singularities occur at zeroes  $\lambda_k$  for finite volume, while they appear only at branch points (not on the cut) in the infinite volume limit [21].

Such branch points are termed the Lee-Yang edge singularities. The Lee-Yang edge singularities have a strong influence, as the closest singularities to the real axis, on the

behaviors of thermodynamic quantities for the real values of  $\lambda$ . They can also be regarded as critical points in the complex plane [37], and thermodynamic quantities become singular with the critical exponents characterized by the Lee-Yang edge singularities. In order to investigate what the edge singularities are like in the vicinity of the CP, we resort to an effective theory reflecting the phase structure of QCD [38]. This model is constructed based on the tricritical point (TCP) in the  $\mu$ - $T$  plane in the chiral limit, which has the upper critical dimension equal to 3, and thus its mean field description is expected to be valid up to a logarithmic correction. It provides some interesting physics in the vicinity of the tricritical point for vanishing quark mass  $m$ , and of the CP for small  $m$ . We make use of this model to investigate the nature in the complex  $\mu$  plane. Thermodynamic singularities in the complex  $\mu$  plane have been studied by Stephanov in terms of the random matrix theory [21]. In the present paper, we pay more attention to the influence of the singularities on the real  $\mu$  axis.

When one introduces complex  $\mu$ , the order parameter also becomes complex and so does the effective potential. Its  $\mu$  dependence is quite intricate in the complex case. The above stated model, however, allows to analyze the complex potential. By focusing on the real part of the potential, we explicitly trace its extrema. In the vicinity of the singularity, their movements show different behaviors depending on where they pass. From its behaviors, we identify where the Stokes lines are located. We also see along the Stokes line that the critical exponent associated with the gap of  $\text{Im } \Omega$  around the singular point differ from that on the real axis. The chiral susceptibility and quark number susceptibility in the complex  $\mu$  plane are also discussed. By moving  $\text{Re } \mu$  with fixed  $\text{Im } \mu$ , the complex susceptibilities show a distinct behavior between  $\text{Im } \mu < \text{Im } \mu^{(s)}$  and  $\text{Im } \mu > \text{Im } \mu^{(s)}$ , where  $\mu^{(s)}$  denotes the singular point in the complex  $\mu$  plane. We trace the peak of the complex susceptibilities. It turns out that the chiral susceptibility develops a peak at a location in agreement with the real part of the singular point in the vicinity of the CP. As a reminiscence of the singularity, the location of the peak of both the susceptibilities on the real axis shows the same temperature dependence as that of  $\text{Re } \mu^{(s)}$ .

In the following section, after a brief explanation of the model, we see how the effective potential looks above, on and below temperature of the CP for various values of real  $\mu$ . We then move to the complex  $\mu$  plane, and investigate the singularities. Chiral and quark number susceptibilities are discussed in connection with the singularities. In section 3,

we explicitly study the extrema of the complex effective potential and discuss the Stokes lines. The chiral and quark number susceptibilities in the complex plane are also discussed. Summary is presented in section 4.

## II. EDGE SINGULARITIES

We investigate the edge singularities of QCD in the complex  $\mu$  plane. For this purpose, we resort to some effective theory describing the phase structure of QCD around the critical point. In the present paper, we adopt a model proposed by Hatta-Ikeda [38]. Although this model is based on the mean field, it is interesting in the sense that the inter-relationship between the TCP and the CP indicates characteristic behaviors of the phase structure.

### A. Effective potential and CP

In this subsection, let us briefly explain the model which we deal with in the paper. We consider  $N_f = 2$  case. In the chiral limit, there exists a TCP at finite temperature and density. The TCP is connected to a critical point at  $\mu = 0$ , which is in the same universality class as 3-d O(4) spin mode [40]. And a first order line goes down from the TCP toward lower temperature side. When quark mass  $m$  is introduced, the critical line is absent, and the surviving first order line terminates at a critical point (CP). This CP can be described by fluctuations of the sigma meson and is expected to share the same universality with 3-d Ising model [4]. Since the upper critical dimension of the tricritical point is equal to 3, the TCP in QCD phase diagram can be described by a mean field theory up to a logarithmic correction. As far as  $m$  is small, the universal behavior around the CP is also expected to be described in the mean field framework. Let us briefly explain the model [38] in the following.

Starting with the Landau-Ginzburg potential, which incorporates only the long wavelength contribution

$$\Omega_{LG} = -m\sigma + \frac{a}{2}\sigma^2 + \frac{b}{4}\sigma^4 + \frac{c}{6}\sigma^6, \quad (2)$$

one expands it around the TCP ( $a = b = m = 0$ ) assuming  $a$  and  $b$  as a linear function of  $\mu$  and  $T$ ,

$$a(T, \mu) = C_a \tilde{t}_3 + D_a \tilde{\mu}_3, \quad b(T, \mu) = C_b \tilde{t}_3 + D_b \tilde{\mu}_3, \quad (3)$$

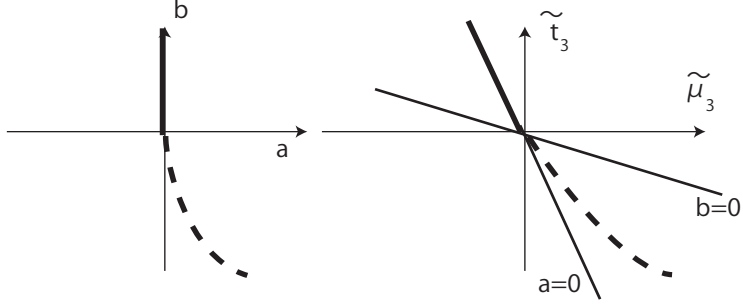


FIG. 1: Mapping of the phase diagram from  $(a, b)$ -plane to  $(\tilde{\mu}_3, \tilde{t}_3)$ -plane. Thick solid (broken) lines indicate a second order critical lines (first order phase transition lines).

where  $\tilde{\mu}_3 = \mu - \mu_3$  ( $\tilde{t}_3 = T - T_3$ ), and  $(\mu_3, T_3)$  denotes temperature and chemical potential at the TCP. A coefficient  $c$  in Eq. (2) is assumed to be constant at the TCP. Coefficients  $C_a, D_a, C_b$  and  $D_b$  in Eq. (3) are constrained to some extent from the structure around the TCP. Positivity of  $C_a$  ( $C_a > 0$ ) is determined from  $a(T, \mu) > 0$  (the symmetric phase) for  $\tilde{t}_3 > 0$  at  $\tilde{\mu}_3 = 0$ , and similarly  $D_a > 0$  is from  $\tilde{\mu}_3 > 0$  at  $\tilde{t}_3 = 0$ . As illustrated in Fig. 1, a second order phase transition line ( $a = 0, b \geq 0$ ) in Eq.(2) is mapped to a straight line  $\tilde{t}_3 = -(D_a/C_a) \tilde{\mu}_3$  ( $\tilde{\mu}_3 \leq 0$  and  $\tilde{t}_3 \geq 0$ ). Moreover, a first order line ( $a = 3b^2/(16c)$ ), existing in the region  $a > 0$  and  $b < 0$  and tangential to  $a = 0$  at the origin in the  $a$ - $b$  plane, is expected to be mapped into the region  $\tilde{\mu}_3 > 0$  and  $\tilde{t}_3 < 0$  and tangential to the straight line  $a = 0$  at the TCP. This is realized when the followings hold

$$C_b D_a - C_a D_b > 0, \quad C_a, C_b, D_a, D_b > 0, \quad (4)$$

where the left condition implies that the linear transformation from  $(a, b)$  to  $(\tilde{\mu}_3, \tilde{t}_3)$  keeps the orientation.

By switching on  $m$ , the condition for the CP to exist at  $T = T_E$  and  $\mu = \mu_E$

$$\frac{\partial \Omega(T_E, \mu_E, \sigma_0)}{\partial \sigma} = \frac{\partial^2 \Omega(T_E, \mu_E, \sigma_0)}{\partial \sigma^2} = \frac{\partial^3 \Omega(T_E, \mu_E, \sigma_0)}{\partial \sigma^3} = 0 \quad (5)$$

leads to the coefficients

$$a(T_E, \mu_E) = \frac{9b(T_E, \mu_E)^2}{20c}, \quad -b(T_E, \mu_E) = \frac{5}{54^{1/5}} c^{3/5} m^{2/5}, \quad (6)$$

and expectation value of  $\sigma$

$$\sigma_0 = \sqrt{\frac{-3 b(T_E, \mu_E)}{10c}}. \quad (7)$$

The CP is deviated from the TCP as follows;

$$T_E - T_3 = -\frac{5D_a c^{3/5}}{(54)^{1/5} (C_b D_a - C_a D_b)} m^{2/5}, \quad (8)$$

$$\mu_E - \mu_3 = \frac{5C_a c^{3/5}}{(54)^{1/5} (C_b D_a - C_a D_b)} m^{2/5}. \quad (9)$$

It is noted that with the condition Eq. (4),  $T_E < T_3$  and  $\mu_E > \mu_3$  hold.

Expanding  $\Omega(T, \mu, \sigma)$  around  $\Omega(T_E, \mu_E, \sigma_0)$ , we obtain thermodynamic potential around the CP given by

$$\Omega(T, \mu, \sigma) = \Omega(T_E, \mu_E, \sigma_0) + A_1 \hat{\sigma} + A_2 \hat{\sigma}^2 + A_3 \hat{\sigma}^3 + A_4 \hat{\sigma}^4, \quad (10)$$

where  $\hat{\sigma} = \sigma - \sigma_0$ . This is the potential we use in the present paper.

The coefficients  $A_i$  are given as follows as a function of  $T$  and  $\mu$ .

$$\begin{aligned} A_1 &= (C_a \sigma_0 + C_b \sigma_0^3) \tilde{t}_E + (D_a \sigma_0 + D_b \sigma_0^3) \tilde{\mu}_E \\ A_2 &= \frac{1}{2} (C_a + 3C_b \sigma_0^2) \tilde{t}_E + \frac{1}{2} (D_a + 3D_b \sigma_0^2) \tilde{\mu}_E \\ A_3 &= \{C_b \tilde{t}_E + D_b \tilde{\mu}_E\} \sigma_0 \\ A_4 &= -\frac{b(T_E, \mu_E)}{2} + \frac{1}{4} (C_b \tilde{t}_E + D_b \tilde{\mu}_E), \end{aligned} \quad (11)$$

where  $\tilde{t}_E \equiv T - T_E$  and  $\tilde{\mu}_E \equiv \mu - \mu_E$ .

The stability  $A_4 > 0$  of the potential (10) gives

$$\tilde{\mu}_E > \frac{2b(T_E, \mu_E) - C_b \tilde{t}_E}{D_b}. \quad (12)$$

It is checked if this stability condition is fulfilled in the following calculations.

Before discussing the properties of the model in the complex  $\mu$  plane, it would be better to see what this model is like in the real  $\mu$  case. This will also be helpful in order to discuss the Stokes line in the following section. Figures 2 and 3 indicate typical behaviors of  $\Omega$  at temperature around the CP. Here we chose the following numerical values for simplicity,

$$x_m = m^{1/5} = 0.2, \quad C_a = 0.1, \quad C_b = D_a = D_b = c = 1.0. \quad (13)$$

and the same values for these parameters are used for the calculations throughout the paper. The left panel of Fig. 2 indicates the behavior of a first order phase transition for a negative value of  $\tilde{t}_E (= -0.2)$ . The values of  $\tilde{\mu}_E \equiv \mu - \mu_E$  are chosen to be 0.054, 0.0555, 0.058, 0.06 from bottom to top. Note that at  $\tilde{t}_E = -0.2$ , a first order phase transition occurs at

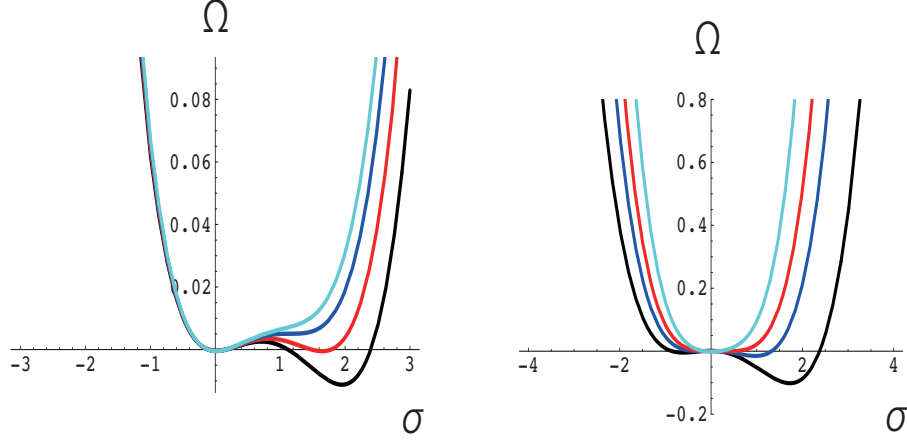


FIG. 2: Behaviors of  $\Omega$  for  $\tilde{t}_E \equiv T - T_E < 0$  (left) and  $\tilde{t}_E = 0$  (right).  $C_a = 0.1$  and  $x_m = m^{1/5} = 0.2$ . The other parameters are  $C_b = D_a = D_b = c = 1.0$ . Left: For  $\tilde{t}_E = -0.2$ , the values of  $\tilde{\mu}_E \equiv \mu - \mu_E$  are chosen to be 0.054, 0.0555 (red line: phase transition point), 0.058, 0.06 from bottom to top. Right: For  $\tilde{t}_E = 0$ , the value of  $\tilde{\mu}_E$  is chosen to be  $-0.1, -0.05, 0$  (red line: CP) and 0.1.

$\tilde{\mu}_E = 0.0555$  (red line). In the right panel, the behaviors at  $\tilde{t}_E = 0$  are shown ( $\tilde{\mu}_E$  is chosen to be  $-0.1, -0.05, 0$  and 0.1 from bottom to top). The critical point corresponds to  $\tilde{\mu}_E = 0$  (red line).

In the left panel of Fig. 3, behaviors of  $\Omega$  for positive value of  $\tilde{t}_E (= 0.2)$  are shown, where  $\tilde{\mu}_E$  is chosen to be  $-0.05, -0.0222$ , and  $-0.001$ . At  $\tilde{t}_E = 0.2$ ,  $\Omega$  develops an approximately flat minimum at  $\tilde{\mu}_E = -0.0222$  (red line). The right panel indicates the inverse curvature of  $\Omega$  at the global minimum as a function of  $\tilde{\mu}_E$ , which develops a peak at  $\tilde{\mu}_E = -0.0222$ .

## B. Edge singularities

Let us now move to the complex  $\mu$  plane. Using the potential in Eq. (10), the instability of the extrema occurs at such  $\sigma$  that

$$\frac{\partial \Omega}{\partial \sigma} = 0, \quad \frac{\partial^2 \Omega}{\partial \sigma^2} = 0 \quad (14)$$

are simultaneously satisfied. Namely,

$$A_1 + 2A_2\sigma + 3A_3\sigma^2 + 4A_4\sigma^3 = 0, \quad 2A_2 + 6A_3\sigma + 12A_4\sigma^2 = 0.$$

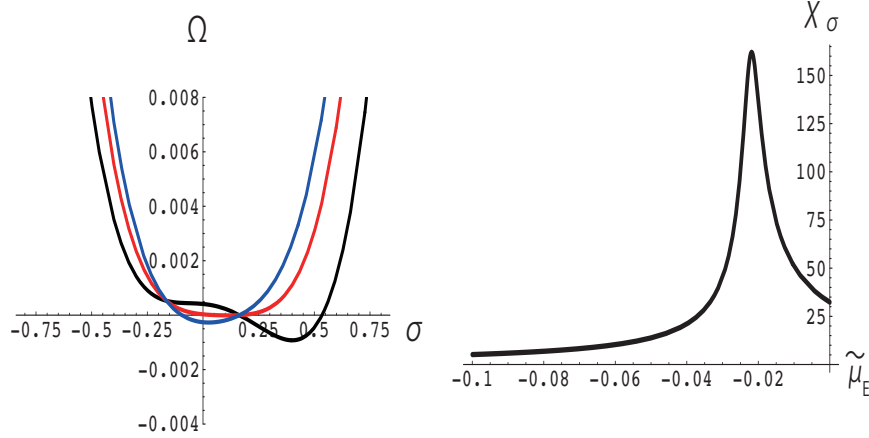


FIG. 3: Behaviors of  $\Omega$  for  $\tilde{t}_E > 0$  (left). Left: For  $\tilde{t}_E = 0.2$ , the value of  $\tilde{\mu}_E$  is chosen to be  $-0.05$ ,  $-0.0222$  (red line: crossover), and  $-0.001$ . Right: the inverse curvature at the global minimum of  $\Omega$  as a function of  $\tilde{\mu}_E$  for  $\tilde{t}_E = 0.2$ .

This occurs when the former cubic equation has vanishing discriminant.

$$-4a_1^3a_3 + a_1^2a_2^2 - 4a_0a_2^3 + 18a_0a_1a_2a_3 - 27a_0^2a_3^2 = 0, \quad (15)$$

where

$$a_0 = 4A_4, \quad a_1 = 3A_3, \quad a_2 = 2A_2, \quad a_3 = A_1. \quad (16)$$

Using the coefficients  $A_i$  in Eq. (11), the discriminant Eq. (15) is solved as a function of  $\tilde{\mu}_E$  and  $\tilde{t}_E$ .

For  $\tilde{t}_E = 0.2$  (Fig. 3), for example, the discriminant Eq. (15) yields four roots such as

$$\tilde{\mu}_E = -0.3857 \text{ (i)}, \quad -0.0538 \text{ (ii)}, \quad -0.0222 \pm 0.00254 i \text{ (iii)}. \quad (17)$$

The stability condition of the potential Eq.(12) gives  $\tilde{\mu}_E > -0.3801$  for  $\tilde{t}_E = 0.2$ , and thus the solution (i) is excluded. In the case (ii), an inflection point is located at  $\sigma = -0.07602$ . This point has nothing to do with the phase transition[42]. The remaining solutions (iii), with their real part satisfying the stability condition, can be identified as a pair of complex singularities at  $\tilde{t}_E = 0.2$  associated with the CP at  $\tilde{t}_E = 0$ . Singularities of type (iii) are denoted by  $\tilde{\mu}_E^{(s)}$ , and we focus on these hereafter.

The left panel of Fig. 5 indicates the locations of  $\tilde{\mu}_E^{(s)}$  in the complex  $\tilde{\mu}_E$  plane for various values of temperature ( $\tilde{t}_E \geq 0$ ). Temperatures are chosen to be  $\tilde{t}_E = T - T_E =$



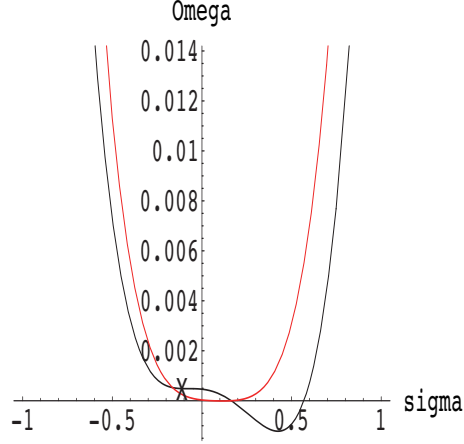


FIG. 4: Potential  $\Omega$ , Eq.(10), for  $\tilde{t}_E = 0.2$ . Two values  $\tilde{\mu}_E$  are chosen. Black line:  $\tilde{\mu}_E = -0.0538$ , where  $\Omega' = \Omega'' = 0$  is fulfilled at  $\sigma = -0.07602$  ( $\times$ ). Red line:  $\tilde{\mu}_E = -0.0222$ , which is equivalent to the real part of (iii) in Eq.(17).

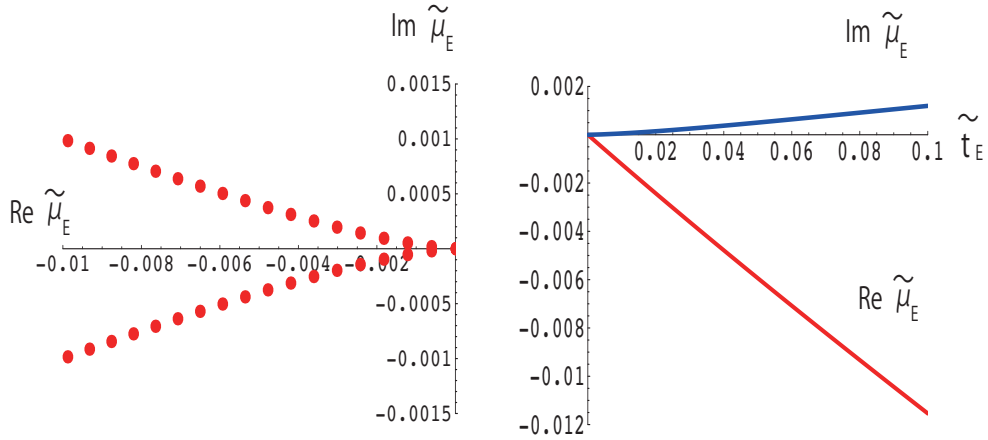


FIG. 5: Left: Singularities in the complex  $\tilde{\mu}_E = \mu - \mu_E$  plane. Temperatures are chosen to be  $\tilde{t}_E = T - T_E = 0, 0.005, 0.01, 0.15, 0.02 \dots 0.09$ . Right: The  $\tilde{t}_E$ -dependence of  $\text{Re } \tilde{\mu}_E^{(s)}$  (red) and  $\text{Im } \tilde{\mu}_E^{(s)}$  (blue).  $\text{Re } \tilde{\mu}_E^{(s)}$  is linear in  $\tilde{t}_E$ , while  $\text{Im } \tilde{\mu}_E^{(s)}$  behaves as  $\tilde{t}_E^{3/2}$  [36].

0, 0.005, 0.01, 0.15, 0.02  $\dots$  0.09. At  $\tilde{t}_E = 0$ , the singularity of the CP appears on the real  $\tilde{\mu}_E$  axis (the origin in the figure). For  $\tilde{t}_E > 0$ , edge singularities appearing in pairs deviate from the real  $\tilde{\mu}_E$ -axis as  $\tilde{t}_E$  increases. The  $\tilde{t}_E$ -dependence of  $\text{Re } \tilde{\mu}_E^{(s)}$  and  $\text{Im } \tilde{\mu}_E^{(s)}$  is shown in the right panel. The real part depends linearly on  $\tilde{t}_E$ , while the imaginary one behaves as  $\tilde{t}_E^{\beta\delta}$  with  $\beta\delta = 3/2$  as expected [21].

In comparison to the result in Ref.[21], we translate the behavior of the singularities in

the  $\tilde{\mu}_E$  plane to that in the  $\mu^2$  plane. For this we need the location of the tricritical point, which is however unknown in this frame work. By putting some appropriate numbers for the tricritical point  $\mu_3$ , we could plot the singularities in the complex  $\mu^2$  plane.  $\text{Re } \mu = \text{Re } \tilde{\mu}_E + \mu_0$  and  $\text{Im } \mu = \text{Im } \tilde{\mu}_E$ . Here,  $\mu_0$  is given in terms of the coefficients  $C_i$ 's and  $\mu_3$ ;

$$\mu_0 = \frac{5C_a c^{3/5}}{(54)^{1/5}(C_b D_a - C_a D_b)} m^{2/5} + \mu_3. \quad (18)$$

The singularities deviate from the real  $\mu^2$  axis as  $\tilde{t}_E$  increases from 0 in the same way as those in Fig. 5, since a mapping from  $\tilde{\mu}_E$  to  $\mu^2$  is a conformal one.

### C. Crossover

Since the singular points move away from the real  $\mu$  axis for positive values of  $\tilde{t}_E$ , substantial quantities like the chiral susceptibility show no singular behavior on the real axis, but the reminiscence of the singularity appears as crossover. At temperatures close to the CP ( $\tilde{t}_E \gtrsim 0$ ), it would then be natural to identify  $\text{Re } \tilde{\mu}_E^{(s)}$  as the location of the crossover on the real  $\mu$  axis [21]. In the example, Eq. (17), at  $\tilde{t}_E = 0.2$ ,  $\Omega$  for  $\tilde{\mu}_E = \text{Re } \tilde{\mu}_E^{(s)} = -0.0222$  looks as shown in Fig. 4 (red line), and the chiral susceptibility  $\chi_\sigma$  becomes maximal at the value in agreement with  $\text{Re } \tilde{\mu}_E^{(s)}$  as was shown in the right panel of Fig. 3, where  $\chi_\sigma$  is given by inverse curvature of the effective potential  $\Omega(\sigma)$  at the global minimum  $\bar{\sigma}$

$$\chi_\sigma = -\frac{\partial^2 \Omega(\bar{\sigma}(m), m)}{\partial m^2} = \frac{1}{\left. \frac{\partial^2 \Omega(\sigma)}{\partial \sigma^2} \right|_{\bar{\sigma}}}. \quad (19)$$

The  $\tilde{t}_E$ -dependence of  $\chi_\sigma$  as a function of  $\tilde{\mu}_E$  is plotted in the left panel of Fig. 6. The peak of the curve shifts away from  $\tilde{\mu}_E = 0$  as  $\tilde{t}_E$  increases, and its location are in agreement with the values of  $\text{Re } \tilde{\mu}_E^{(s)}$  for each  $\tilde{t}_E$ .

The right panel of Fig. 6 indicates the locations of the thus identified crossover for various values of temperature ( $\tilde{t}_E > 0$ ), together with the locations of the first order phase transition for  $\tilde{t}_E < 0$ . Red symbols indicate first order phase transition points, green ones do the locations of the crossover, and the CP is located at the origin.

### D. Quark number susceptibility

At the CP, fluctuations of the quark number as well as the heat capacity become singular in the same exponent as that of the chiral susceptibility [38, 39]. For  $\tilde{t}_E > 0$ , the singularity

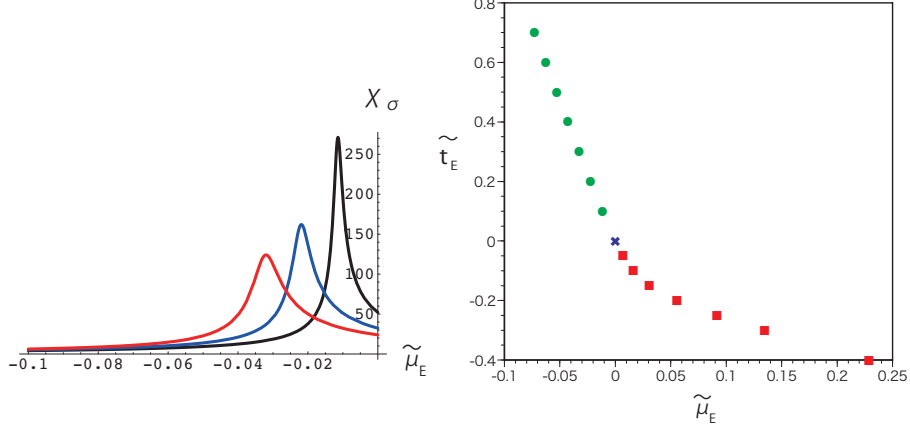


FIG. 6: Left:  $\chi_\sigma$  as a function of  $\tilde{\mu}_E$ .  $\tilde{t}_E = 0.1$ (black), 0.2 (blue) and 0.3 (red). Right: Phase diagram around the CP. The horizontal (vertical) axis is  $\tilde{\mu}_E$  ( $\tilde{t}_E$ ), and the origin ( $\times$ ) is the location of the CP.  $x_m = 0.2$ . Red symbols indicate first order phase transition points, and green ones do the locations of the crossover, which are in agreement with the real parts of the singularities,  $\text{Re } \tilde{\mu}_E^{(s)}$ .

in the complex plane makes an effect on the locations of the crossover in a slightly different way. The quark number susceptibility is defined by

$$\chi_q = -\frac{\partial^2 \Omega(\bar{\sigma}, \mu)}{\partial \mu^2}, \quad (20)$$

where  $\bar{\sigma}$  is the value of  $\sigma$  at the global minimum of the potential in (10). Figure 7 shows  $\chi_q$  as a function of  $\tilde{\mu}_E$  ( $\tilde{t}_E = 0$  (black), 0.02 (red), 0.04 (green) and 0.06 (blue)). At the CP ( $\tilde{t}_E = 0$ ),  $\chi_q$  diverges at  $\tilde{\mu}_E = 0$ , and away from the CP ( $\tilde{t}_E > 0$ ),  $\chi_q$  develops a finite amount of peak, whose height becomes smaller as  $\tilde{t}_E$  increases. Locations of the peak of  $\chi_q$  and  $\chi_\sigma$  are approximately the same, but deviate from each other as temperature increases from the CP temperature, reflecting the difference of explicit dependence of  $\Omega' = \partial \Omega / \partial \sigma$  on  $m$  and  $\mu$ , respectively;

$$\chi_\sigma = \frac{\left(\frac{\partial \Omega'}{\partial m}\right)^2}{\frac{\partial^2 \Omega(\bar{\sigma})}{\partial \sigma^2}} = \frac{1}{\frac{\partial^2 \Omega(\bar{\sigma})}{\partial \sigma^2}}, \quad \chi_q = \frac{\left(\frac{\partial \Omega'}{\partial \mu}\right)^2}{\frac{\partial^2 \Omega(\bar{\sigma})}{\partial \sigma^2}}. \quad (21)$$

This will be discussed again in connection with the complex susceptibilities in III C.

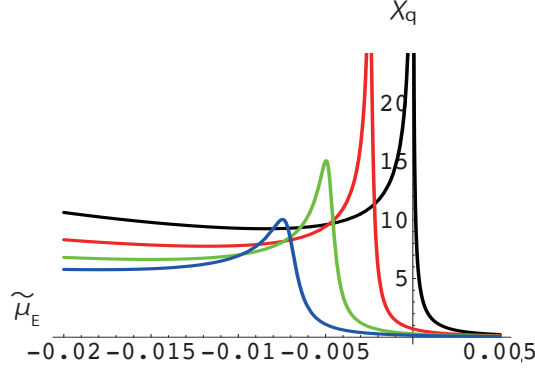


FIG. 7: Quark number susceptibility as a function of  $\tilde{\mu}_E$  for four values of temperature ( $\tilde{t}_E = 0$  (black), 0.02 (red), 0.04 (green) and 0.06 (blue)).

### III. ANALYTIC CONTINUATIONS

In this section, we consider the analytic continuation of the extrema of the effective potential. By tracing them in the complex  $\mu$  plane, the Stokes lines are identified, which reflects the analytic structure around the branch points. It will also be seen that the crossover phenomenon of  $\chi_\sigma$  on the real  $\mu$  axis reflects the characteristics of the singular behavior of  $\chi_\sigma$  in the complex plane. It is understood that although we focus on the behaviors in the complex upper-half  $\tilde{\mu}_E$  plane, those also occur in the lower-half plane in the complex conjugate manner.

#### A. Analytic continuation of extrema of the effective potential

The Stokes line is understood as a curve to which the Lee-Yang zeros accumulate as shown in Eq. (1). When the phase transition occurs, zeros accumulate onto the critical point by which two phases are separated on the real axis. As the parameter is analytically continued from the one phase to the other, the corresponding global minimum of the potential is also analytically continued. In the present system, for  $\tilde{t}_E = 0$ , the critical point exists at  $\tilde{\mu}_E = 0$ , while for  $\tilde{t}_E > 0$ , the singular point is shifted into the complex plane.

Let us consider  $\tilde{t}_E > 0$ , and move  $\tilde{\mu}_E$ , as shown in the left panel of Fig. 8, from a point on the real axis ( $\tilde{\mu}_E > 0$ ) to the other side at  $\tilde{\mu}_E < 0$  by changing  $\theta$  from 0 to  $\pi$  in  $\tilde{\mu}_E = \rho e^{i\theta}$  for a fixed value of  $\rho$ . The singular point is located at  $\tilde{\mu}_E^{(s)} = \rho^{(s)} e^{i\theta^{(s)}}$ . Firstly, we choose  $\rho > \rho^{(s)}$ . In the course of the variation of  $\theta$ , a minimum of  $\text{Re } \Omega(\sigma)$  analytically continued

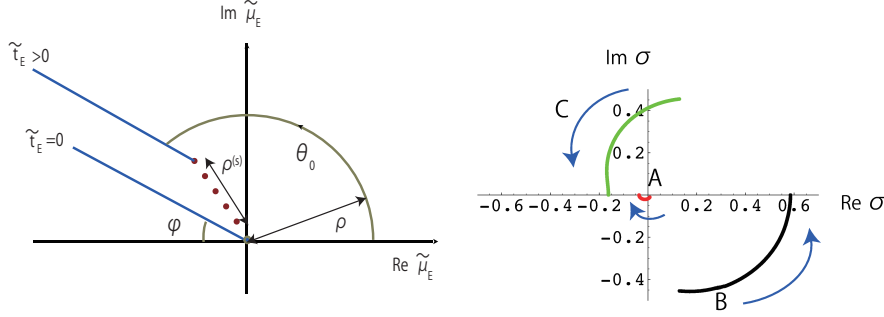


FIG. 8: Left: Stokes line (blue) in the complex  $\tilde{\mu}_E$  plane. The singular point  $\tilde{\mu}_E^{(s)}$  for  $\tilde{t}_E = 0$  is located at the origin, while for  $\tilde{t}_E > 0$  one of complex pair of  $\tilde{\mu}_E^{(s)}$  is shifted to the negative  $\text{Re } \tilde{\mu}_E$  direction in the upper half plane. Angle  $\varphi$  is defined from the negative side of  $\text{Re } \tilde{\mu}_E$  axis. See text for detail. Right: Behaviors of three extrema of  $\text{Re } \Omega$  in the complex  $\sigma$  plane as  $\tilde{\mu}_E = \rho e^{i\theta}$  varies from  $\theta = 0$  to  $\theta = \pi$  ( $\rho = 0.05$ ) [36].

from  $\tilde{\mu}_E > 0$  jumps discontinuously, at some value of  $\theta$  ( $\equiv \theta_0$ ), to the one continued from the other side of  $\tilde{\mu}_E < 0$  in the complex  $\sigma$  plane. The location where such transition occurs corresponds to crossing the Stokes line in the complex  $\tilde{\mu}_E$  plane. From the argument in Introduction, the two values of  $\text{Re } \Omega(\sigma)$  become equal at this point. That is, the Stokes lines are given by

$$\text{Re } \Omega(\sigma_+) = \text{Re } \Omega(\sigma_-), \quad (22)$$

where  $\sigma_+(\sigma_-)$  is the location of the extremum analytically continued from  $\tilde{\mu}_E > 0$  ( $\tilde{\mu}_E < 0$ ). In order to explicitly see how this occurs, we take  $\tilde{t}_E = 0.1$ . At this temperature, the singular points are located at  $\tilde{\mu}_E^{(s)} = -0.0115 \pm i 0.0012$  and thus  $\rho^{(s)} = 0.0116$ . The right panel of Fig. 8 shows behaviors of three extrema of  $\text{Re } \Omega$  in the complex  $\sigma$  plane as  $\theta$  varies from 0 to  $\pi$  with fixed value of  $\rho$  ( $= 0.05$ ). For  $\theta = 0$ ,  $\text{Re } \Omega$  develops three extrema at  $\sigma = 0.0108$  (A) and  $\sigma = 0.12910 - i 0.4544$  (B) and  $0.12910 + i 0.4544$  (C), each of which is located at the initial point of the arrows denoted by A, B and C, respectively. The arrows in the figure indicate the direction of the movement of the three as  $\theta$  varies from 0 to  $\pi$ . The extremum A, which is a global minimum for  $\theta = 0$ , ends up with negative small value of  $\sigma = -0.0366$  at  $\theta = \pi$ , while B does with the real axis at  $\sigma = 0.5848$ , which is identified as the global minimum of  $\Omega$  for  $\theta = \pi$  from its shape (see Fig. 3). So the two extrema A and B are associated with the global minimum of  $\Omega$  for real  $\mu$ , the phase for  $\tilde{\mu}_E > 0$  and the one

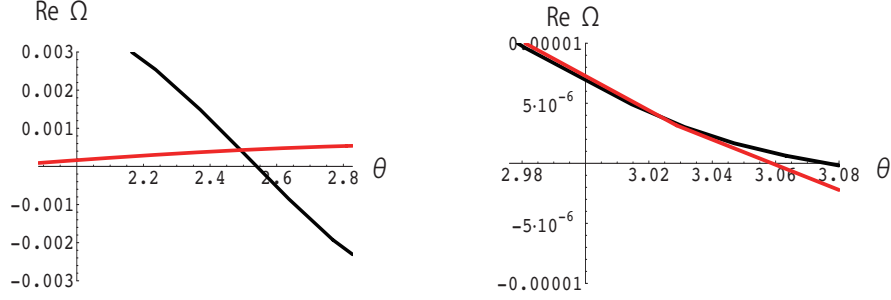


FIG. 9: Behaviors of  $\text{Re } \Omega$  for the two extrema A (red) and B (black) as  $\tilde{\mu}_E = \rho e^{i\theta}$  varies for fixed  $\rho$ ,  $\tilde{t}_E = 0.1$  and  $\rho^{(s)} = 0.0116$ . Left:  $\rho = 0.05$ . The two values of  $\text{Re } \Omega$  agree at  $\theta_0 = 2.492$ . Right:  $\rho = \rho^{(s)}$ . The two values of  $\text{Re } \Omega$  agree at  $\theta_0 = 3.038$ . Only the regions around  $\theta_0$  are shown.

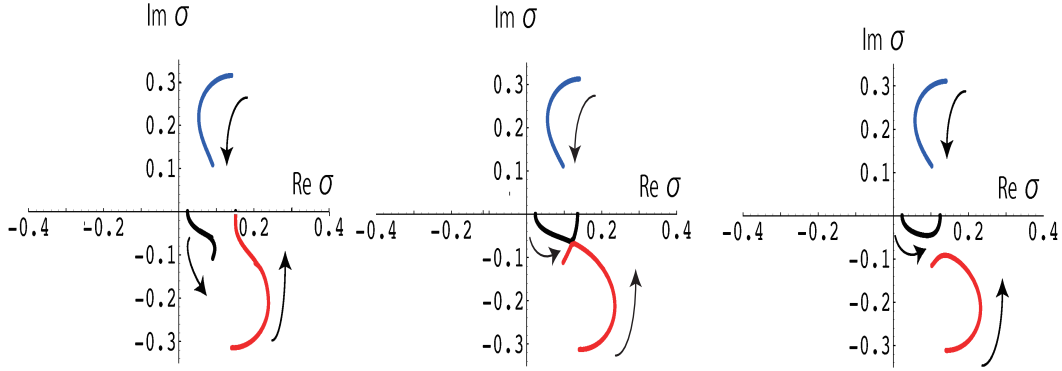


FIG. 10: Behaviors of the three extrema around the singular point of  $\text{Re } \Omega$  in the complex  $\sigma$  plane as  $\tilde{\mu}_E = \rho e^{i\theta}$  varies from  $\theta = 0$  to  $\pi$ . Left:  $\rho = 0.012$ , middle:  $\rho = \rho^{(s)} = 0.0116$ , right:  $\rho = 0.0113$ . Temperature  $\tilde{t}_E$  is set to 0.1. The minimum corresponding to the singularity at  $\tilde{\mu}_E = -0.0115 + i 0.0012$ , fulfilling the condition Eq. (14), is attained at  $\sigma = 0.1219 - i 0.0653 \equiv \sigma^{(s)}$ , where two trajectories meet together in the middle panel.

for  $\tilde{\mu}_E < 0$ , respectively, while the extremum C is not associated with the phase transition. In the left panel in Fig. 9, the behavior of  $\text{Re } \Omega$  for the two extrema A and B is shown as a function of  $\theta$ . The two values agree at  $\theta_0 = 2.492$ , where their slopes show a discontinuity in accordance with the analogy of two dimensional Coulomb gas.

It is then interesting to see how the trajectories of the extrema of  $\text{Re } \Omega$  change in the vicinity of the singular point. For  $\tilde{t}_E = 0.1$ , the minimum of  $\text{Re } \Omega$  for  $\tilde{\mu}_E$  at the singularity,  $\tilde{\mu}_E^{(s)} = -0.0115 + i 0.0012$ , i.e., fulfilling the condition Eq. (14), is attained at  $\sigma = 0.1219 - i 0.0653 \equiv \sigma^{(s)}$ . Figure 10 shows the behaviors of the three extrema of  $\text{Re } \Omega$  in the complex

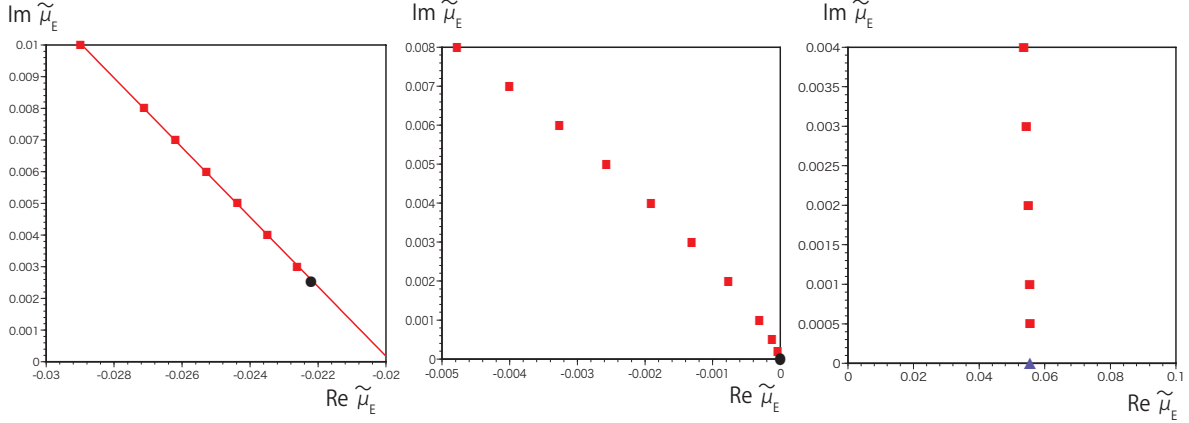


FIG. 11: Locations of the Stokes line (red) in complex  $\tilde{\mu}_E$  plane, which are calculated by  $\text{Re } \Omega$  for the two extrema. Left:  $\tilde{t}_E$  is chosen to be 0.2. Black symbol denotes the location of the singular point  $\tilde{\mu}_E^{(s)} = -0.02221 + i 0.00254$ . It is clearly seen that thus identified points sit on a straight line with the slope  $-1.09 \pm 0.02$ . Middle:  $\tilde{t}_E = 0$ . Singularity corresponding the CP is situated at the origin. In this case the Stokes line emanates from the origin with  $\varphi = \pi/2$ . Right:  $\tilde{t}_E = -0.2$ . A first order phase transition is located at  $\tilde{\mu}_E = 0.05553$  (blue triangle). From this point, a Stokes line goes out upright ( $\varphi = \pi/2$ ).

$\sigma$  plane for three different values of  $\rho$ ;  $\rho = 0.012$  ( $> \rho^{(s)}$ ),  $0.0116$  ( $= \rho^{(s)}$ ) and  $0.0113$  ( $< \rho^{(s)}$ ). For  $\rho = \rho^{(s)}$ , the two minima A and B approach each other and meet together at  $\sigma^{(s)}$  as shown in the middle panel of Fig.10. In this case,  $\text{Re } \Omega$  of the two trajectories behaves as shown in the right panel of Fig. 9. A smooth encounter of the two trajectories occurs at  $\theta_0 = 3.0384$  ( $= 0.9672\pi$ ), whose value is indeed in agreement with the location of the singularity  $\tilde{\mu}_E^{(s)} = -0.0115 + i 0.0012$ .

As  $\rho$  varies passing  $\rho^{(s)}$  near  $\tilde{\mu}_E^{(s)}$ , the two trajectories make a rearrangement. In the leftmost panel of Fig.10 ( $\rho > \rho^{(s)}$ ), three trajectories behave like those in the right panel of Fig. 8, i.e., A (B) is the global minimum for  $\tilde{\mu}_E > 0$  ( $\tilde{\mu}_E < 0$ ). In contrast with this, for  $\rho = 0.012$  ( $< \rho^{(s)}$ ), only a single extremum A is associated with analytic continuation from  $\tilde{\mu}_E > 0$  to  $\tilde{\mu}_E < 0$ , as shown in the rightmost figure in Fig.10. That is, no encounter with the Stokes line is found in this case.

As another case of  $\rho > \rho^{(s)}$ , let us comment a behavior when  $\rho$  is chosen to be a specific value  $\rho = 0.04322$ . In this case, two extrema B and C (instead of A and B) meet together at  $\sigma = -0.0795229$  for  $\theta = \pi$  ( $\tilde{\mu}_E = -0.04322$ ), where the condition  $\Omega' = \Omega'' = 0$  is fulfilled

for  $\tilde{t}_E=0.1$ . This corresponds to the extremum ( $\times$ ) irrelevant to the phase transition as discussed in Fig. 4 and the footnote.

## B. Stokes lines

In the case of  $\tilde{t}_E > 0$ , therefore, the Stokes line runs for  $\rho > \rho^{(s)}$ . The left panel of Fig. 11 indicates how the Stokes line emanates from the singular point  $\tilde{\mu}_E^{(s)}$  in the complex  $\tilde{\mu}_E$  plane. Red filled symbols indicate the locations which are calculated in the way described above, i.e., by choosing several value of  $\rho$ , tracing the trajectories of the extrema and checking the behaviors of  $\text{Re } \Omega$ . For  $\tilde{t}_E = 0.2$ , the singular point is located at  $\tilde{\mu}_E^{(s)} = -0.02221 + i 0.00254$  (black symbol in the Figure). It is seen that the Stokes line is aligned on a straight line, which is tilted with angle  $\varphi = \pi/4$  from an axis parallel to the negative axis of  $\text{Re } \tilde{\mu}_E$ . This is in agreement with analytic consideration shown in Appendix A 2 [43].

As  $\tilde{t}_E$  decreases to 0,  $\tilde{\mu}_E^{(s)}$  approaches the origin, and the angle  $\varphi$  shows a increasing tendency. The middle panel of Fig. 11 shows the Stokes line emanating from the origin for  $\tilde{t}_E = 0$ . This behavior is in agreement with  $\varphi = \pi/2$  as shown in Appendix A 4. For  $\tilde{t}_E < 0$ , a first order phase transition is located on the positive  $\tilde{\mu}_E$  axis. In the right panel of Fig. 11, we show the case for  $\tilde{t}_E = -0.2$ , where a first order phase transition is located at  $\tilde{\mu}_E = 0.05553$  (blue triangle). From this point, a Stokes line goes out upright with  $\varphi = \pi/2$  (see Appendix A 3 [44]). In recent Monte Carlo study [41] of low temperature and high density QCD, the distribution of the Lee-Yang zeros have been calculated, and it looks similar to the behavior in the right panel of Fig. 11, suggesting a possible first order phase transition.

To close this subsection, we briefly discuss  $\text{Re } \Omega$  and  $\text{Im } \Omega$  along the Stokes line. On the Stokes line, two values of  $\text{Re } \Omega$  continued from real  $\tilde{\mu}_E$  axis agree (Eq. (22)). In the left panel of Fig. 12, such  $\text{Re } \Omega$  is plotted as a function of  $\text{Im } \tilde{\mu}_E$  for  $\tilde{t}_E = 0.2$ , which increases linearly. In contrast to this,  $\text{Im } \Omega$  shows a gap on the Stokes line (at the singular point, the gap vanishes). The behavior of the discontinuity  $\Delta \text{Im } \Omega \equiv \text{Im } \Omega(\sigma_+) - \text{Im } \Omega(\sigma_-)$  is shown in the right panel of Fig. 12. The gap grows as

$$\Delta \text{Im } \Omega \sim (\text{Im } \tilde{\mu}_E - \text{Im } \tilde{\mu}_E^{(s)})^{3/2}, \quad (23)$$

where  $\text{Im } \tilde{\mu}_E$  denotes the imaginary part of the points on the Stokes line (see the left panel in Fig. 11). The exponent  $3/2$  comes from the behavior of  $\sigma_+$  near the singularity



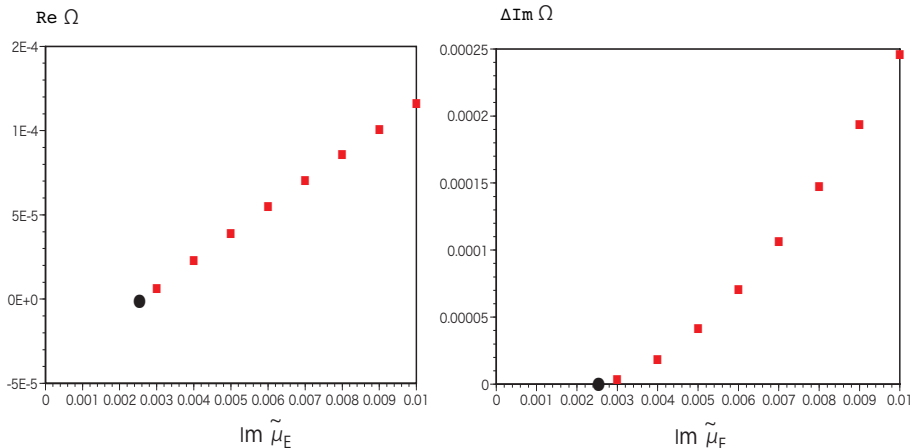


FIG. 12:  $\text{Re } \Omega$  (left) and  $\Delta \text{Im } \Omega$  (right) as a function of  $\text{Im } \tilde{\mu}_E$  along the Stokes line for  $\tilde{t}_E = 0.2$ . Black filled symbol indicates the singular point.  $\text{Re } \Omega$  increases linearly with  $\text{Im } \tilde{\mu}_E$  (left), and  $\Delta \text{Im } \Omega$  vanishes at the singular point (right).

$\text{Re } \sigma_+ \sim (\text{Im } \tilde{\mu}_E - \text{Im } \tilde{\mu}_E^{(s)})^{1/2}$ , which reflects the fact that the critical exponents for the edge singularity are, in general, different from the usual ones on the real axis [26, 37]. In the case of  $\tilde{t}_E = 0$ , we have  $\text{Re } \sigma_+ \sim (\text{Im } \tilde{\mu}_E)^{1/3}$  and  $\Delta \text{Im } \Omega \sim (\text{Im } \tilde{\mu}_E)^{4/3}$  (see Appendix B). This corresponds in the Ising case to the magnetization behaving like  $(h - h^{(s)})^{1/2}$  near the singular point  $h^{(s)}$  on the imaginary magnetic field  $h$  axis for  $T > T_c$  and  $\sim h^{1/\delta}$  for  $T = T_c$  ( $\delta = 3$  for the mean field case). It is also noted that at a Lee-Yang zero for finite volume, the discontinuity is like  $\Delta \text{Im } \Omega = (2k + 1)\pi$  ( $k$  : integer) per volume.

### C. Susceptibility in the complex plane

The crossover behaviors of the susceptibilities on the real  $\tilde{\mu}_E$  axis reflects the structure of the singularity in the complex plane. Let us then study the behaviors of the susceptibilities in the complex plane. We fix  $\text{Im } \tilde{\mu}_E$  and move  $\text{Re } \tilde{\mu}_E$  by separating the region into two, one is  $0 \leq \text{Re } \tilde{\mu}_E \leq \text{Re } \tilde{\mu}_E^{(s)}$  and the other  $\text{Re } \tilde{\mu}_E^{(s)} \leq \text{Re } \tilde{\mu}_E$ . In this subsection, we plot  $\text{Re } \Omega'' = (\text{Re } \chi_\sigma)^{-1}$  and  $(\text{Re } \chi_q)^{-1}$  so that they become vanishing at the singular point  $\tilde{\mu}_E^{(s)}$ , rather than diverging  $\chi_\sigma$  and  $\chi_q$ .

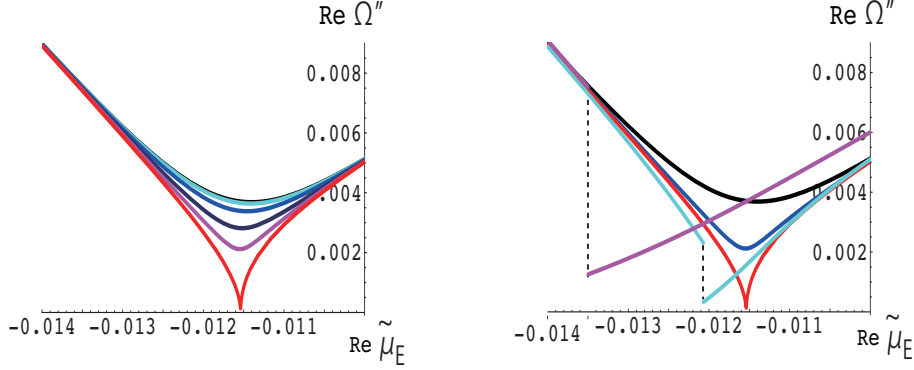


FIG. 13: Behaviors of  $\text{Re } \Omega''$  as a function of  $\text{Re } \tilde{\mu}_E$  for fixed values of  $\text{Im } \tilde{\mu}_E$  for  $\tilde{t}_E = 0.1$ , where  $\tilde{\mu}_E^{(s)} = -0.011538 + i 0.0011946$ . Left:  $\text{Im } \tilde{\mu}_E = 0, 0.0002, 0.0005, 0.001$  and  $0.0011946 (= \text{Im } \tilde{\mu}_E^{(s)})$ . Right:  $\text{Im } \tilde{\mu}_E = 0, 0.001, 0.0011946 (= \text{Im } \tilde{\mu}_E^{(s)}), 0.002$  and  $0.004$ . For  $\text{Im } \tilde{\mu}_E > \text{Im } \tilde{\mu}_E^{(s)}$ ,  $\text{Re } \Omega''$  shows a discontinuity (broken lines) when  $\text{Re } \tilde{\mu}_E$  crosses the Stokes line.

1.  $0 \leq \text{Im } \tilde{\mu}_E \leq \text{Im } \tilde{\mu}_E^{(s)}$

For  $\tilde{t}_E = 0.1$ , the left panel in Fig. 13 indicates  $\text{Re } \Omega''$  as a function of  $\text{Re } \tilde{\mu}_E$  for fixed values of  $\text{Im } \tilde{\mu}_E$  ( $0 \leq \text{Im } \tilde{\mu}_E \leq \text{Im } \tilde{\mu}_E^{(s)}$ ).  $\text{Re } \Omega''$  develops a minimum, which, as  $\text{Im } \tilde{\mu}_E \rightarrow \text{Im } \tilde{\mu}_E^{(s)}$ , approaches zero at  $\text{Re } \tilde{\mu}_E = \text{Re } \tilde{\mu}_E^{(s)}$ , where  $\tilde{\mu}_E^{(s)} = -0.011538 + i 0.0011946$ . Figure 14 indicates the location of the minimum of  $\text{Re } \Omega''$  in the complex  $\tilde{\mu}_E$  plane for various values of  $\tilde{t}_E$  (0.05, 0.1, 0.15, 0.2). The minimum shows a slight  $\text{Im } \tilde{\mu}_E$  dependence (the deviation between  $\text{Re } \tilde{\mu}_E^{(s)}$  and  $\text{Re } \tilde{\mu}_E$  of the minimum point on the real axis is at most around 2 % in the case under consideration). As  $\text{Im } \tilde{\mu}_E \rightarrow \text{Im } \tilde{\mu}_E^{(s)}$ , it approaches the singular point  $\tilde{\mu}_E^{(s)}$ , and winds around a bit in the vicinity of  $\tilde{\mu}_E^{(s)}$ , which reflects the behaviors of the minima of  $\text{Re } \Omega$  around  $\tilde{\mu}_E^{(s)}$  (see Fig. 10). In contrast, the location of the minimum of the inverse real part of the quark number susceptibility  $(\text{Re } \chi_q)^{-1}$  depend more on  $\tilde{\mu}_E$  than that of  $\text{Re } \Omega''$  as shown in Fig. 14 (the deviation between  $\text{Re } \tilde{\mu}_E^{(s)}$  and  $\text{Re } \tilde{\mu}_E$  of the minimum point on the real axis is around 10 % for  $\tilde{t}_E = 0.2$ ). It is stressed that the crossover phenomena on the real axis are originated from the same complex singularity, and that  $\chi_\sigma$  reflects the singularity in the complex plane more directly than  $\chi_q$  does.

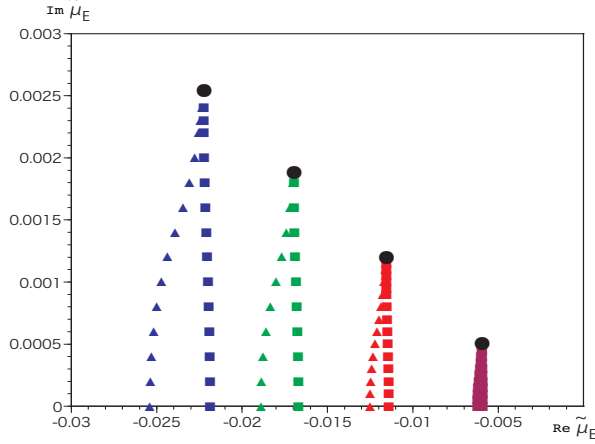


FIG. 14: The  $\tilde{t}_E$  dependence of the location of the minimum of  $\text{Re } \Omega''$  (square symbol) and that of  $(\text{Re } \chi_q)^{-1}$  (triangle) in the complex  $\tilde{\mu}_E$  plane. Only the locations in the region  $0 \leq \text{Im } \tilde{\mu}_E \leq \text{Im } \tilde{\mu}_E^{(s)}$  for each  $\tilde{t}_E$  are plotted. Filled black symbols indicate  $\tilde{\mu}_E^{(s)}$  for four different temperatures  $\tilde{t}_E = 0.05$  (violet),  $0.1$  (red),  $0.15$  (green),  $0.2$  (blue).

### 2. $\text{Im } \tilde{\mu}_E^{(s)} \leq \text{Im } \tilde{\mu}_E$

In the region  $\text{Im } \tilde{\mu}_E^{(s)} \leq \text{Im } \tilde{\mu}_E$ , varying  $\text{Re } \tilde{\mu}_E$  comes across the Stokes line in the vicinity of  $\tilde{\mu}_E^{(s)}$ . The right panel in Fig. 13 indicates the behaviors of  $\text{Re } \Omega''$  as a function of  $\text{Re } \tilde{\mu}_E$  for fixed values of  $\text{Im } \tilde{\mu}_E$ . Figure 13 includes also those for  $0 \leq \text{Im } \tilde{\mu}_E \leq \text{Im } \tilde{\mu}_E^{(s)}$  as a comparison. For  $\text{Im } \tilde{\mu}_E^{(s)} \leq \text{Im } \tilde{\mu}_E$ ,  $\text{Re } \Omega''$  changes discontinuously at a value of  $\text{Re } \tilde{\mu}_E$  corresponding to the Stokes line as shown in Fig. 13 (broken lines). The gap of the discontinuity  $\Delta \text{Re } \Omega'' \equiv \text{Re } \Omega''(\sigma_+) - \text{Re } \Omega''(\sigma_-)$  on the Stokes line varies depending on how far the point is from the singular point. The left panel in Fig. 15 indicates that  $\Delta \text{Re } \Omega''$  increases linearly as a function of  $\rho = |\tilde{\mu}_E|$  for  $\tilde{t}_E = 0.1$ , where  $\tilde{\mu}_E$  is on the Stokes line. At  $\rho = \rho^{(s)} \equiv |\tilde{\mu}_E^{(s)}|$ ,  $\Delta \text{Re } \Omega''$  is vanishing.

### 3. On the real axis

Let us turn to behaviors on the real  $\tilde{\mu}_E$  axis. The right panel in Fig. 15 indicates the  $\tilde{t}_E$  dependence of the location of the minimum of  $\text{Re } \Omega''$  (square) and that of  $(\text{Re } \chi_q)^{-1}$  (circle) on the real  $\tilde{\mu}_E$  axis. It is seen that both the locations depend linearly on  $\tilde{t}_E$  coming from the linear dependence of  $\text{Re } \tilde{\mu}_E^{(s)}$ . It is noted that the difference between  $\text{Re } \tilde{\mu}_E^{(s)}$  and the

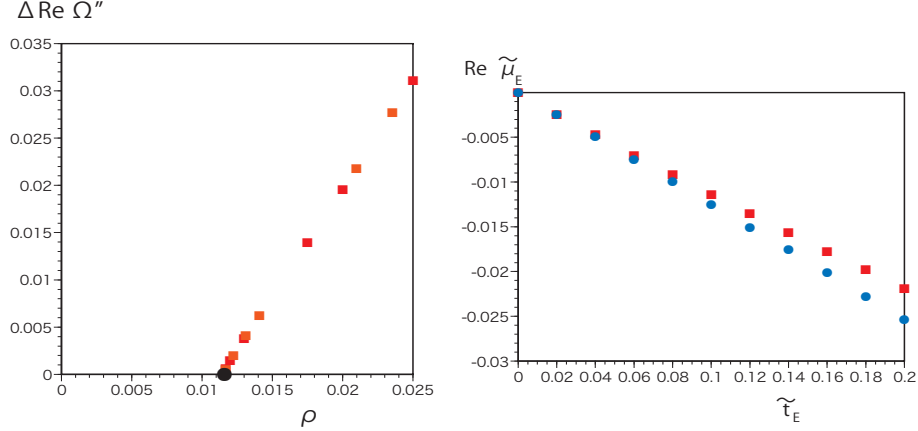


FIG. 15: Left: The gap of  $\text{Re } \Omega''$ ,  $\Delta \text{Re } \Omega''$ , on the Stokes line, increases linearly as a function of distance  $\rho$ , where  $\rho = |\tilde{\mu}_E|$  at a point on the Stokes line and  $\rho^{(s)} = \left| \tilde{\mu}_E^{(s)} \right|$  (filled black symbol).  $\tilde{t}_E = 0.1$ . Right: The  $\tilde{t}_E$  dependence of the location of the minimum of  $\text{Re } \Omega''$  (square) and that of  $(\text{Re } \chi_q)^{-1}$  (circle) on the real axis ( $\text{Im } \tilde{\mu}_E = 0$ ). A linear fit works well for both the quantities.

locations of the minimum of  $\text{Re } \Omega''$  is invisibly small.

The susceptibility in the complex plane also behaves with the critical exponent characterized by the edge singularity. On the real  $\tilde{\mu}_E$  axis, it is given by  $1/\delta - 1 = -2/3$ , while in the complex plane, it changes to  $-1/2$  (see Appendix B).

#### IV. CONCLUSION

We have discussed the thermo-dynamic singularities in the complex chemical plane in QCD at finite temperature and finite densities. For this purpose, we have adopted an effective theory incorporating fluctuations around the CP. Singularities in the complex chemical potential plane are identified as unstable points of the extrema of the complex effective potential. At CP temperature, the singularity is located on the real  $\mu$  axis, and above CP temperature it moves away from the real axis leaving its reminiscence as a crossover. The location of the chiral susceptibility peak agrees with  $\text{Re } \tilde{\mu}_E^{(s)}$  in the vicinity of the singularity.

Simplicity of the model allows us to explicitly deal with the complex potential as a function of the complex order parameter and complex values of  $\mu$ . We have had a close look at the behavior of the extrema of  $\text{Re } \Omega(\sigma)$  in the complex order parameter plane. It is seen that two relevant extrema make a rearrangement at the singular point under the variation

of  $\mu$  around the singularity in the complex plane. It is also clearly seen that the Stokes line is located in different ways depending on above, on and below CP temperature, which provide information as to where the Lee-Yang zeros are located for finite volume. Along the Stokes line,  $\text{Im } \Omega$  shows a gap, and the gap increases with the exponent characterized by the Lee-Yang edge singularity.

We have considered the chiral and quark number susceptibilities in the complex plane. As a reminiscence of the singularity, the locations of the peaks of both the susceptibilities on the real axis exhibit a linear dependence on  $\tilde{t}_E$ , reflecting the  $\tilde{t}_E$  dependence of  $\text{Re } \tilde{\mu}_E^{(s)}$  in the complex plane. The susceptibility in the complex plane also behaves with the critical exponent characterized by the edge singularity.

Some remarks are in order. (i) The framework discussed here is not sufficient to make a realistic prediction by fixing some physical scale. For this, a study on more realistic model beyond the mean field framework would be desirable. (ii) This model focuses on the vicinity of the TCP and CP, and physics concerning the imaginary chemical potential is beyond the scope of the present paper. (iii) For the sake of concrete calculations we have chosen some appropriate values for the parameters (such as  $C_a$  etc.) appearing in the potential in Eq. (11). The universal behaviors discussed in the complex plane are irrelevant to such a choice. (iv) It may be worth while quantifying what is described here. In [23], the QCD singularities  $N_f = 2$  QCD with staggered quarks have been investigated by having a look at the effective potential with respect to the plaquette variable. In order to having a more contact with the present paper, some refinement of the computation would be necessary.

## Acknowledgments

The authors are grateful to H. Kouno for useful discussion concerning the susceptibilities. They also thanks H. Aoki, M. Imachi and M. Tachibana for useful discussion. S. E. is in part supported by Grants-in-Aid of the Japanese Ministry of Education, Culture, Sports, Science and Technology (No. 23540259).

## Appendix A: Stokes line

In this appendix, we analytically consider the angle  $\varphi$  of the Stokes line in the vicinity of the TCP, the critical point ( $m = 0$ ), the first order phase transition point for  $\tilde{t}_3 < 0$  ( $m = 0$ ) and the CP ( $\tilde{t}_E < 0$ ), respectively.

### 1. Stokes line for the TCP

Firstly, we consider the case  $T = T_3$  ( $\tilde{t}_3 = 0$ ). In Eq. (2) with  $m = 0$  and the coefficients in Eq. (3), the symmetric phase for  $\tilde{\mu}_3 > 0$  and the broken one for  $\tilde{\mu}_3 < 0$  compete in the vicinity of the TCP. In the broken phase,  $\Omega$  develops two degenerate minima for  $|\tilde{\mu}_3| \ll 1$  such as

$$\bar{\sigma} \approx \pm e^{-i\pi/4} \sqrt{\frac{D_a}{c} \tilde{\mu}_3^{1/4}} = \pm (-\tilde{\mu}_3)^{1/4}, \quad (\text{A1})$$

while  $\bar{\sigma} = 0$  in the symmetric phase. Therefore

$$\Omega(\tilde{\mu}_3) \begin{cases} \approx -i \frac{D_a^{3/2}}{3\sqrt{c}} \tilde{\mu}_3^{3/2} = \frac{1}{3} (-\tilde{\mu}_3)^{3/2} & (\tilde{\mu}_3 < 0) \\ = 0 & (\tilde{\mu}_3 > 0), \end{cases} \quad (\text{A2})$$

where the second equality for  $\tilde{\mu}_3 < 0$  holds with our choice of the parameters in Eq.(13). Thus the condition Eq.(22) gives a tilted Stokes line with angle  $\varphi = \pi/3$ .

### 2. Stokes line for the critical point ( $m = 0$ )

In the massless case, the critical line runs for  $\tilde{t}_3 > 0$ , and the condition for this is  $a = 0$  in Eq. (2), i.e.,

$$\tilde{\mu}_3 = -\frac{C_a}{D_a} \tilde{t}_3 \equiv \tilde{\mu}_3^c. \quad (\text{A3})$$

In the vicinity of  $\mu_3^c$ , the global minimum and  $\Omega$  behave as

$$\bar{\sigma} \begin{cases} \propto \frac{1}{\sqrt{\tilde{t}_3}} (\tilde{\mu}_3^c - \tilde{\mu}_3)^{1/2} & (\tilde{\mu}_3 < \tilde{\mu}_3^c) \\ = 0 & (\tilde{\mu}_3 > \tilde{\mu}_3^c), \end{cases} \quad (\text{A4})$$

and

$$\Omega(\tilde{\mu}_3) \begin{cases} \propto -\frac{1}{\tilde{t}_3} (\tilde{\mu}_3^c - \tilde{\mu}_3)^2 & (\tilde{\mu}_3 < \tilde{\mu}_3^c) \\ = 0 & (\tilde{\mu}_3 > \tilde{\mu}_3^c), \end{cases} \quad (\text{A5})$$

respectively. The exponent of  $\Omega$  differs from that in the previous case ( $\tilde{t}_3 = 0$ ), which causes the change of  $\varphi$ . The Stokes line is thus tilted with angle  $\varphi = \pi/4$  in the vicinity of each critical point on the critical line.

### 3. Stokes lines for $\tilde{t}_3 < 0$ ( $m = 0$ )

In the case of  $\tilde{t}_3 < 0$ , a first order phase transition occurs at  $\tilde{\mu}_3 = \mu_3^c$ , where

$$\mu_3^c = \frac{1}{3D_b^2} \left( 8cD_a - 3C_bD_b\tilde{t}_3 - 4\sqrt{4c^2D_a^2 - 3cD_b(C_bD_a - C_aD_b)\tilde{t}_3} \right). \quad (\text{A6})$$

In the vicinity of the  $\mu_3^c$ , the global minimum and  $\Omega$  behave as

$$\bar{\sigma} = \begin{cases} \bar{\sigma}_0 + \bar{\sigma}_1(\tilde{\mu}_3 - \tilde{\mu}_3^c) & (\tilde{\mu}_3 < \tilde{\mu}_3^c) \\ 0 & (\tilde{\mu}_3 > \tilde{\mu}_3^c), \end{cases} \quad (\text{A7})$$

and

$$\Omega(\tilde{\mu}_3) = \begin{cases} d_1(\tilde{\mu}_3 - \tilde{\mu}_3^c) & (\tilde{\mu}_3 < \tilde{\mu}_3^c) \\ 0 & (\tilde{\mu}_3 > \tilde{\mu}_3^c), \end{cases} \quad (\text{A8})$$

respectively, where  $\bar{\sigma}_0$ ,  $\bar{\sigma}_1$  and  $d_1$  are coefficients, which depend intricately on  $C_a$  etc. in Eq.(3). The linear dependence of  $\Omega$  in the broken phase yields  $\varphi = \pi/2$ . It suggests in finite volume that the Lee-Yang zeros at low temperatures and high densities are located parallel to the imaginary  $\mu$  axis. This is in agreement with the recent Monte Carlo result obtained by utilizing the reduction formula of the reduced Dirac matrix [41].

### 4. Stokes line for the CP ( $\tilde{t}_E = 0$ )

At  $\tilde{t}_E = 0$  and in the vicinity of the CP ( $m \neq 0$ ), the global minimum and  $\Omega$  behave as follows.

$$\bar{\sigma} \approx \begin{cases} \sigma_0 - \bar{\sigma}_1 (-\tilde{\mu}_E)^{1/3} & (\tilde{\mu}_E < 0) \\ \sigma_0 - \bar{\sigma}_1 (\tilde{\mu}_E)^{1/3} & (\tilde{\mu}_E > 0), \end{cases} \quad (\text{A9})$$

$$\Omega(\tilde{\mu}_E) \approx \begin{cases} d_0 (-\tilde{\mu}_E)^{4/3} & (\tilde{\mu}_E < 0) \\ d_0 (\tilde{\mu}_E)^{4/3} & (\tilde{\mu}_E > 0). \end{cases} \quad (\text{A10})$$

Here  $\sigma_0$  is given in Eq. (7), and  $\bar{\sigma}_1$  and  $d_0$  are coefficients, which depend on  $C_a$  etc. in Eq.(3). In this case,  $\varphi = \pi/2$ .

## Appendix B: Critical exponent of the chiral susceptibility

1. on the real  $\tilde{\mu}_E$  axis ( $\tilde{t}_E = 0$ )

Here, the behavior of the chiral susceptibility around the CP is discussed. Since the singularity of the CP at  $\tilde{t}_E = 0$  is located at the origin in the complex  $\tilde{\mu}_E$  plane, behaviors of the chiral susceptibility around the CP are given by fluctuations of  $\sigma$  at the global minimum of  $\Omega$  in the vicinity of  $\tilde{\mu}_E^{(s)} = 0$ .

True vacuum  $\bar{\sigma}$  which gives the global minimum of  $\Omega(T, \mu, \sigma)$  is obtained by solving  $\frac{\partial \Omega}{\partial \sigma} = 0$ , namely,

$$A_1 + 2A_2\hat{\sigma} + 3A_3\hat{\sigma}^2 + 4A_4\hat{\sigma}^3 = 0. \quad (\text{B1})$$

This equation is cubic and it can be analytically solved. Ignoring higher-order terms in  $\tilde{\mu}_E$  around the CP, one obtains

$$\bar{\sigma} \simeq \sigma_0 + \left( \frac{D_a\sigma_0 + D_b\sigma_0^3}{2b(T_E, \mu_E)} \right)^{1/3} |\tilde{\mu}_E|^{1/3}. \quad (\text{B2})$$

The curvature of  $\Omega$  for true vacuum is calculated as follows:

$$\frac{\partial^2 \Omega(\bar{\sigma}(\tilde{\mu}_E), \mu)}{\partial \sigma^2} \simeq -6b(T_E, \mu_E) \left( \frac{D_a\sigma_0 + D_b\sigma_0^3}{2b(T_E, \mu_E)} \right)^{2/3} |\tilde{\mu}_E|^{2/3}, \quad (\text{B3})$$

where the contributions of the first term ( $\mathcal{O}(|\tilde{\mu}_E|^1)$ ) and second one ( $\mathcal{O}(|\tilde{\mu}_E|^{4/3})$ ) are neglected due to  $|\tilde{\mu}_E| \ll 1$ .

The chiral susceptibility, thus, behaves as

$$\chi_\sigma \sim |\tilde{\mu}_E|^{-2/3} \quad (\text{B4})$$

in the vicinity of the origin in the complex  $\tilde{\mu}_E$  plane.

2. in the complex  $\tilde{\mu}_E$  plane ( $\tilde{t}_E > 0$ )

For  $\tilde{t}_E > 0$  with fixed  $\text{Im } \tilde{\mu}_E = \text{Im } \tilde{\mu}_E^{(s)}$ ,  $\bar{\sigma}$  behaves like

$$\delta\bar{\sigma} \equiv \bar{\sigma} - \sigma^{(s)} \sim (\delta\tilde{\mu}_E)^{1/2}, \quad (\text{B5})$$

in the vicinity of the singular point ( $\delta\tilde{\mu}_E \equiv \tilde{\mu}_E - \tilde{\mu}_E^{(s)}$ ). Similarly to the  $\tilde{t}_E = 0$  case,  $\delta\Omega'' \equiv \Omega''(\bar{\sigma}) - \Omega''(\sigma^{(s)})$  ( $\Omega''(\sigma^{(s)}) = 0$ ) behaves like

$$\begin{aligned} \delta\Omega'' &= 2\delta A_2 + 6\delta(A_3\hat{\sigma}) + 12\delta(A_4\hat{\sigma}^2) \\ &= D_a(\delta\tilde{\mu}_E)^1 + 6\sigma_0 D_b\sigma^{(s)}(\delta\tilde{\mu}_E)^1 + 6\sigma_0 D_b\tilde{\mu}_E^{(s)}(\delta\tilde{\mu}_E)^{1/2} + 12(-b/2)2\sigma^{(s)}(\delta\tilde{\mu}_E)^{1/2} \\ &\sim (\delta\tilde{\mu}_E)^{1/2}, \end{aligned} \quad (\text{B6})$$



leading to

$$\text{Re } \chi_\sigma \sim (\delta\tilde{\mu}_E)^{-1/2}. \quad (\text{B7})$$

- 
- [1] M. Asakawa and K. Yazaki, Nucl. Phys. A **504**, 668 (1989).
- [2] A. Barducci, R. Casalbuoni, S. D. Curtis, R. Gatto and G. Pettini, Phys. Lett. B **231**, 463 (1989).
- [3] M. A. Stephanov, K. Rajagopal, E. Shuryak, Phys. Rev. Lett. **81**, 4816 (1998).
- [4] M. A. Halasz, A. D. Jackson, R. E. Shrock, M. A. Stephanov and J. J. M. Verbaarschot, Phys. Rev. D **58**, 096007(1998).
- [5] J. Berges and K. Rajagopal, Nucl. Phys. B **538**, 215 (1999)
- [6] For a review see K. Fukushima and T. Hatsuda, Rep. Prog. Phys. **74**, 014001 (2011), and see also references therein.
- [7] C. R. Allton, S. Ejiri, S. J. Hands, O. Kaczmarek, F. Karsch, E. Laermann, C. Schmidt and L. Scorzato, Phys. Rev. D **66**, 074507 (2002).
- [8] C. R. Allton, S. Ejiri, S. J. Hands, O. Kaczmarek, F. Karsch, E. Laermann and C. Schmidt, Phys. Rev. D **68**, 014507 (2003).
- [9] C. R. Allton, M. Döring, S. Ejiri, S. J. Hands, O. Kaczmarek, F. Karsch, E. Laermann and K. Redlich, Phys. Rev. D **71**, 054508 (2005).
- [10] R. V. Gavai and S. Gupta, Phys. Rev. D **68**, 034506 (2003).
- [11] M. -P. Lombardo, Nucl. Phys. B (Proc. Suppl.)**83**, 375 (2000).
- [12] P. de Forcrand and O. Philipsen, Nucl. Phys. B **642**, 290 (2002).
- [13] P. de Forcrand and O. Philipsen, Nucl. Phys. B **673**, 170 (2003).
- [14] M. D’Elia and M. -P. Lombardo, Phys. Rev. D **67**, 014505 (2003).
- [15] M. D’Elia and M. -P. Lombardo, Phys. Rev. D **70**, 074509 (2004).
- [16] P. Cea, L. Cosmai, M. D’Elia and A. Papa, J. High Energy Phys. **02** 066 (2007).
- [17] P. Cea, L. Cosmai, M. D’Elia, C. Manneschi and A. Papa, Phys. Rev. D **80**, 034501(2009).
- [18] For a review see S. Muroya, A. Nakamura, C. Nonaka and T. Takaishi, Prog. Theor. Phys. **110**, 615 (2003), and see also references therein.
- [19] S. Ejiri, K. Kanaya and T. Umeda, Prog. Theor. Exp. Phys. **01**, A104 (2012).
- [20] S. Ejiri, Eur. Phys. J. A **49**, 86 (2013).
- [21] M. A. Stephanov, Phys. Rev. D **73**, 094508 (2006).
- [22] V. Skokov, K. Morita and B. Friman, Phys. Rev. D **83**, 071502(R) (2011).

- [23] S. Ejiri and H. Yoneyama, Proceedings of Science (LAT2009) 173 (2009), arXiv:0911.2257[hep-lat].
- [24] C. N. Yang and T.D. Lee, Phys. Rev. **87**, 404 (1952).
- [25] T.D. Lee and C. N. Yang, Phys. Rev. **87**, 410 (1952).
- [26] C. Itzykson, R.B. Pearson and J.B. Zuber, Nucl. Phys. B **220**, 415 (1983).
- [27] I. M. Barbour, S. E. Morrison, E. G. Klepfish, J. B. Kogut and M. -P. Lombardo, Phys. Rev. **D56**, 7063 (1997).
- [28] I. M. Barbour, S. E. Morrison, E. G. Klepfish, J. B. Kogut and M. -P. Lombardo, Nucl. Phys. B (Proc. Suppl.)**60A**, 220 (1998).
- [29] Y. Aoki, F. Csikor, Z. Fodor and A. Ukawa, Phys. Rev. **D60**, 013001 (1999).
- [30] Z. Fodor and S. D. Katz, JHEP **04**, 050 (2004).
- [31] S. Ejiri, Phys. Rev. **D73**, 054502 (2006).
- [32] A. Nakamura and K. Nagata, arXiv:1305.0760 [hep-ph] (2013).
- [33] A. Denblyker, D. Du, Y. Liu, Y. Meurice and H. Zou, Phys. Rev. Lett. **104**, 251601 (2010).
- [34] Y. Liu, and Y. Meurice, Phys. Rev. **D83**, 096008 (2011).
- [35] Z. Gelzer, Y. Liu, Y. Meurice and D. Sinclair, arXiv:1312.3906 [hep-lat].
- [36] S. Ejiri, Y. Shinno, H. Yoneyama, arXiv:1311.6073 [hep-lat].
- [37] M. E. Fisher, Phys. Rev. Lett. **40**, 1610 (1978).
- [38] Y. Hatta and T. Ikeda, Phys. Rev. D **67**, 014028 (2003).
- [39] H. Fujii and M. Ohtani, Phys. Rev. D **70**, 014016 (2004).
- [40] R. D. Pisarski and F. Wilczek, Phys. Rev. **D29**, 338 (2011).
- [41] K. Nagata, S. Motoki, Y. Nakagawa, A. Nakamura and T. Saito, Prog. Theor. Exp. Phys. **01**, A103 (2012)
- [42] Actually, it corresponds to one of the extrema as will be discussed in subsection III A, depicted as (C) in the right panel of Fig. 8. Since this point is misleading from the viewpoint of the singularity, it is stressed as shown in Fig. 4 (cross symbol on the black line). This extremum does not take part in the phase transition.
- [43] In Appendix A 2, the critical line for  $\tilde{t}_3 > 0$  in the  $m = 0$  case is discussed. When  $m$  is small, it is expected that the Stokes line is tilted with the same angle  $\varphi$ .
- [44] The Stokes line is tilted with the same angle  $\varphi$  as far as  $m$  is small.